Green afterglow of Dy^{3+} doped $SrSiO_3$

Bao–gai Zhai, Chao–lai Lu, Jun–shen Li, Ming Yu Li, Lei Cai, Yuan Ming Huang*

School of Mathematics and Physics, Changzhou University, Jiangsu 213164, China

(*Received 12 June 2017; accepted 10 July 2017*)

Dy^{3+} doped strontium metasilicate ($SrSiO_3:Dy^{3+}$) microcrystals were synthesized by solid state reaction process at a temperature of 1300 °C for 3 h. The crystal structure, morphology, chemical composition, photoluminescence spectrum, color coordinates, afterglow spectrum and afterglow decay curve of the synthesized $SrSiO_3:Dy^{3+}$ microcrystals were analyzed using X–ray diffraction, scanning electron microscopy, energy dispersive X–Ray spectroscopy and photoluminescence spectroscopy, respectively. Under the excitation of the 325 nm laser line, the $SrSiO_3:Dy^{3+}$ microcrystals give off intense white light emission. The photoluminescence spectrum of $SrSiO_3:Dy^{3+}$ microcrystals is composed of two characteristic blue emission ($^4F_{9/2}\rightarrow{}^6H_{15/2}$) and the yellow emission ($^4F_{9/2}\rightarrow{}^6H_{13/2}$) of Dy^{3+} ions, whose peaks are located at 485 and 572 nm, respectively. Although no afterglow can be detected after the illumination of the 325 nm laser line, intense green afterglow from $SrSiO_3:Dy^{3+}$ can be observed with naked eyes under the illumination of a high–pressure mercury lamp (175 W). The green afterglow spectrum of $SrSiO_3:Dy^{3+}$ is composed of two sharp peaks with their peaks centered at around 482 and 573 nm, respectively. The afterglow decay curve of the $SrSiO_3:Dy^{3+}$ phosphor exhibits a double exponential decay feature with fitting parameters τ_1 = 24.63 s and τ_2 = 102.49 s. The characteristic emissions of Dy^{3+} in the photoluminescence and afterglow spectra have indicated that Dy dopant acts as the photoluminescent center and the afterglow center.

Keywords: Strontium metasilicate; Afterglow; Photoluminescence; Phosphors; Energy transfer; Electron trap

1. Introduction

Long–lasting phosphorescence, a phenomenon due to the thermal stimulated recombination of holes and electrons at traps, which leave holes or electrons in a long–lived excited state at room temperature, is an interesting phenomenon in which the material persists for a long time after the removal of the excitation source. Based on this intrinsic merit, much interest was aroused in various rare earth ion–doped crystals and glasses for applications as luminous glass, emergency signs, watches and graphic arts, etc. Currently, the best performance of the long–lasting phosphorescence materials are Eu^{2+}–doped alkaline–earth aluminate phosphors, examples of which include green afterglow from Eu^{2+} and Dy^{3+} co–doped $SrAl_2O_4$ [1–5], blue afterglow from Eu^{2+} and Nd^{3+} co–doped $CaAl_2O_4$ [5], and blue–green afterglow from Dy^{3+} doped $BaAl_2O_4$ [6]. Besides the rare–earth doped alkaline–earth aluminates, rare–earth doped alkaline–earth silicates have been extensively researched in recent years as a new generation of long afterglow phosphors due to a growing market for their application in traffic signs, emergency exit routes, decoration, and textile printing [7–10]. Examples include yellow persistent luminescence of $Sr_2SiO_4:Eu^{2+},Dy^{3+}$ [9], $MgSiO_3:Mn^{2+},Nd^{3+}$ [10], $CdSiO_3:Mn^{2+},Tb^{3+}$ [11], white afterglow from $CdSiO_3:Dy^{3+}$ [12], white afterglow from $SrSiO_3:Dy^{3+}$ [13]. Compared with the aluminates, the silicates–based long afterglow phosphors yield much better chemical stability against water along with relatively easier preparation and lower cost in starting materials. In all Dy^{3+} doped $SrSiO_3$ materials, some researchers reported that white–light long afterglow emission was achieved since the afterglow center is identical to the photoluminescence (PL) center, i.e., Dy^{3+} ions [12,13]. It is known that the two main characteristic emissions of Dy^{3+} are in the wavelength range 470–500 nm (blue) and 570–600 nm (yellow), corresponding to the $^4F_{9/2}\rightarrow{}^6H_{15/2}$ and the $^4F_{9/2}\rightarrow{}^6H_{15/2}$ transitions, respectively. The two–colour light emissions can produce white light through an appropriate combination in Dy^{3+}–doped materials.

In this work, we prepared Dy^{3+}–activated $SrSiO_3$ phosphors via the high–temperature solid state reaction method. The structure, particle morphology, chemical composition, PL spectrum, afterglow spectrum and afterglow decay curve of the phosphor were analyzed. It is found that green afterglow can be observed after the illumination of a high–pressure mercury lamp (175 W) for a couple of minutes.

2. Materials and method

$SrSiO_3:Dy^{3+}$ was prepared by the conventional high temperature solid–state reaction. The starting materials were high–purity $SrCO_3$ (0.1 mol), SiO_2 (0.1 mol) and Dy_2O_3 (0.0025 mol). All reagents were provided by Sinopharm Chemical Reagents Co., Ltd. (Shanghai, China). The purity of Dy_2O_3 was 99.99% while all other reagents were in analytical grade. The ratio of Dy^{3+} ions to of Sr^{2+} ions in the starting materials was 5 mol%. After the starting materials had been homogenized thoroughly in a motar, the mixture was sintered in air atmosphere at 1300 °C for 3 h using alumina crucibles with alumina lids followed by subsequent air cooling to room temperature.

The crystal structure of prepared powders was determined by X–ray diffractometer (XRD, D/max 2500 PC, Rigaku Corporation, Japan) using Cu Kα radiation (λ = 0.15405 nm). The voltage applied to the Cu target in the XRD machine was 40 kV. The scanning electron microscope (SEM) analysis was conducted on a SEM machine (S–4800, Hitachi). The accelerating voltage applied to the electron gun in the SEM was 15 kV. The SEM was coupled with a silicon drifted detector as the X–ray analyzer for the energy dispersive X–Ray spectroscopic (EDX) analysis. The PL spectra of the $SrSiO_3:Dy^{3+}$ was recorded at room temperature with a

*Corresponding author. Email: dongshanisland@126.com

spectrophotometer (Tianjin Gangdong Inc., China). A grating with 1200 grooves/mm was installed into the spectrophotometer, the spectral resolution of the spectrophotometer was around 0.2 nm at 500 nm. The excitation wavelength for the PL measurement was the 325 nm emission line from a helium–cadmium laser (Kimmon Koha Co. Ltd., Japan).

3. Results and discussions

3.1 Crystal structure of $SrSiO_3:Dy^{3+}$

The crystal structure of the synthesized compound $SrSiO_3:Dy^{3+}$ was verified using powder XRD technique. Fig. 1 shows the XRD curve of the synthesized compound $SrSiO_3:Dy^{3+}$ with the dopant concentration of 5 mol%. As shown in Fig. 1, the most prominent peaks in the XRD curves are located at 17.527, 24.95, 26.465, 30.626, 25.879, 43.905, 47.592, 51.168 and 54.377 º , respectively. These peaks can be assigned to the Bragg reflections from the planes (002), (020), (021), (022), (203), ($\bar{3}$ 31), (331), (040) and (006) of monoclinic crystal $SrSiO_3$. The standard diffraction data of the monoclinic $SrSiO_3$ (JCPDS card no. 34–0099) are displayed at the bottom of Fig. 1 for comparison. It is obvious that the diffraction peaks of the $SrSiO_3:Dy^{3+}$ phosphor match with those of the standard monoclinic $SrSiO_3$. whose lattice constants are a = 1.234 nm, b = 0.7136 nm, c = 1.088 nm and β = 111.51º. The data in Fig. 1 indicate that the prepared phosphor has the monoclinic $SrSiO_3:Dy^{3+}$ phase via the high–temperature solid state reaction. One can also see in Fig. 1 that the addition of 5 mol% of Dy^{3+} dopant causes no obvious influence in the crystal structure of $SrSiO_3:Dy^{3+}$.

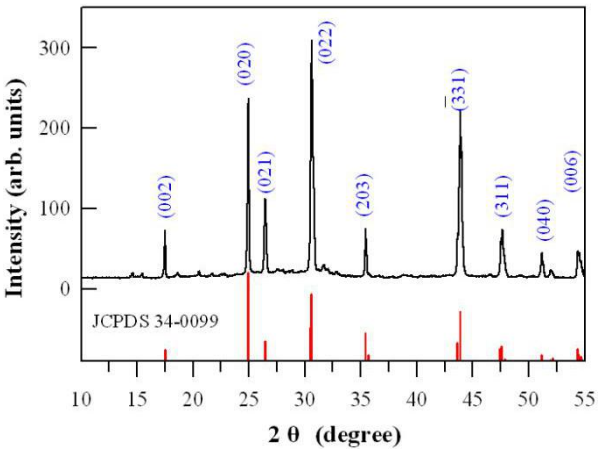

Fig. 1 XRD curve of the $SrSiO_3:Dy^{3+}$ microcrystals. The standard data of monoclinic $SrSiO_3$ (JCPDS 34–0099) are displayed at the bottom for comparison.

Fig. 2(a) depicts the unit cell of monoclinic $SrSiO_3$. The initial structural data of $SrSiO_3$ were taken from Inorganic Crystal Structure Database (ICSD no 32542). It is clear that the unit cell consists 10 Sr sites, 10 Si sites and 30 O sites. The lattice constants of monoclinic $SrSiO_3$ are a = 1.232 nm, b = 0.7139 nm, c = 1.087 nm and β = 111.58º. The space group of monoclinic $SrSiO_3$ is C_2 with the group number of 5. Fig. 2(b) represents the crystal structure of $SrSiO_3$ when viewed along the z axis. It can be seen in Fig. 2(b) that: (i) $SrSiO_3$ consists of SiO_4 tetrahedrons; and (ii) three SiO_4 tetrahedrons in $SrSiO_3$ forms a cyclic $(Si_3O_9)^{6-}$ ring by corner–sharing sharing the O atoms of the three tetrahedrons. The structure with $(Si_3O_9)^{6-}$ ring is the characteristic of monoclinic $SrSiO_3$ [14,15]. Fig. 2(c) represents the crystal structure of $SrSiO_3$ when viewed along the x axis. The Sr atoms occupy three kinds of sites [Sr(1), Sr(2) and Sr(3)], which are surrounded by 8 O atoms with different Sr–O bonding lengths. The structure consists of Sr^{2+} ions and the $(Si_3O_9)^{6-}$ rings alternatively packed along the direction perpendicular to (001). The structure has alternate layers of ternary rings of SiO_4 groups and close–packed Sr atoms stacked along [001]. As viewed in Fig. 2(c), this compound has a four–layer structure although it was reported as a six–layer structure in the literature [14]. The other characteristics in Fig. 2(c) is that a channel is formed around Sr cation in monoclinic $SrSiO_3$. In present case, from the viewpoint of ionic radii, it is reasonable to suggest that the Dy^{3+} ions (0.091nm) are expected to occupy the Sr^{2+} (0.118 nm) sites in the $SrSiO_3$ host and no Dy^{3+} ion is expected to occupy the Si^{4+} sites (0.041 nm) or O^{2-} sites (0.140 nm).

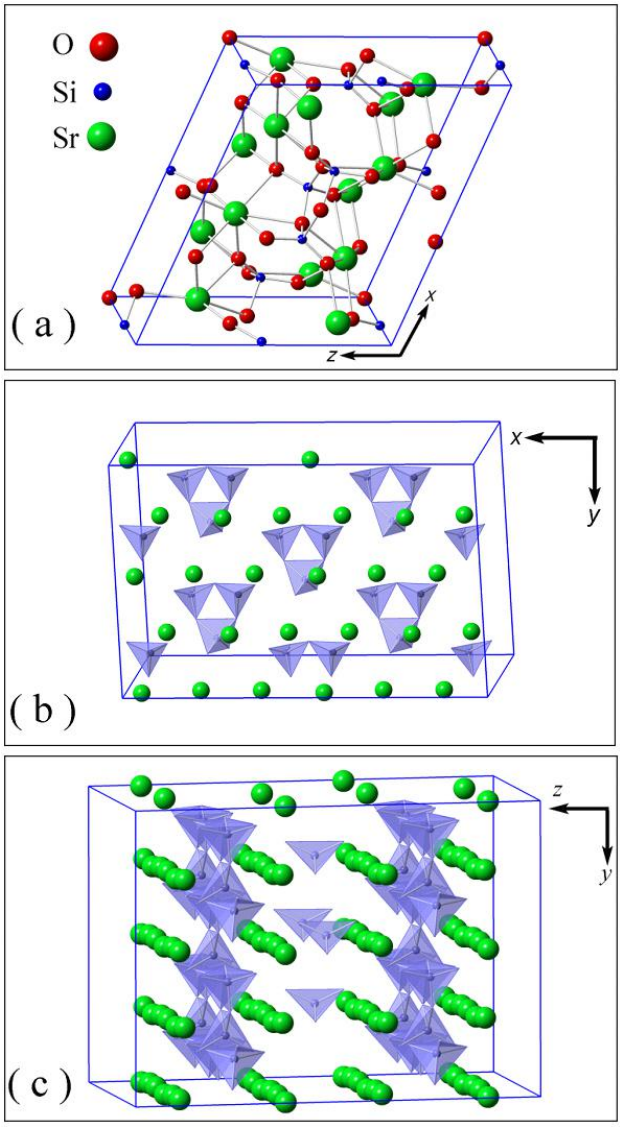

Fig. 2 (a) Unit cell of monoclinic $SrSiO_3$; (b) the crystal structure of $SrSiO_3$ when viewed along the z axis; (c) the crystal structure of $SrSiO_3$ when viewed along the x axis.

3.2 Morphology of $SrSiO_3:Dy^{3+}$

The synthesized $SrSiO_3:Dy^{3+}$ are micrometer–sized particles. Fig. 3(a–c) shows the SEM micrographs of $SrSiO_3:Dy^{3+}$. It is clear that the particles did not have regular shapes. The typical sizes of these irregular particles are several micrometers in dimension. The high temperature in the solid state reaction is responsible for the growth of micrometer–sized particles.

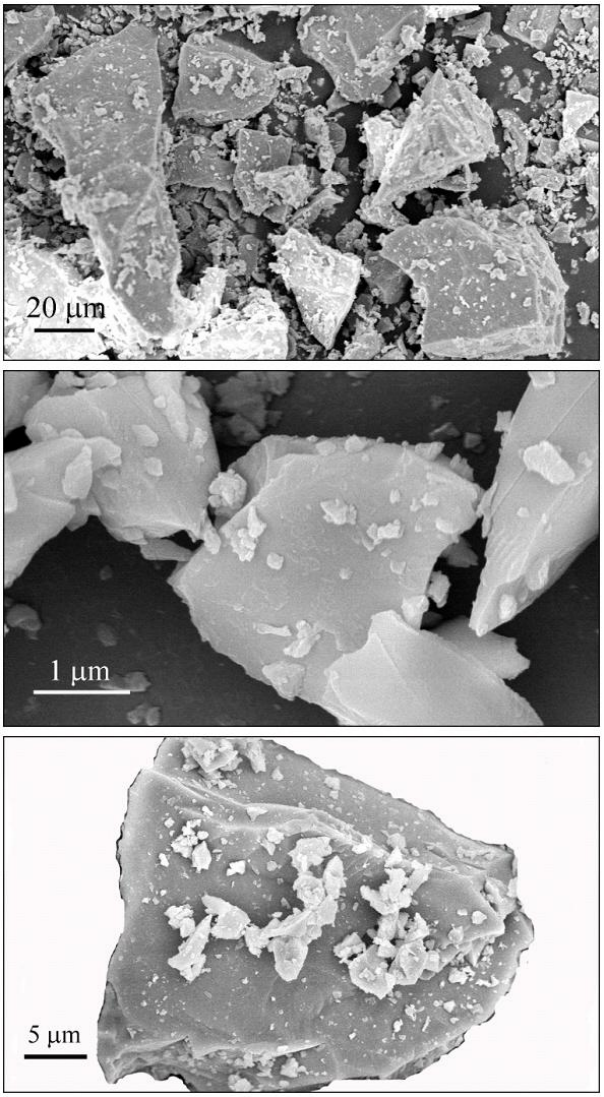

Fig. 3 SEM micrographs of Dy^{3+} doped $SrSiO_3$.

3.3 Chemical compositions of $SrSiO_3:Dy^{3+}$

Fig. 4 depicts the EDX spectrum of the $SrSiO_3:Dy^{3+}$ with the dopant concentration of 5 mol%. As can be seen in Fig. 4, the 3 X–ray emission peaks appear at 0.53, 2.15 and 9.66 keV, which can be attributed to the characteristic X–ray emissions of O($K\alpha_1$), Au($M\alpha_1$) and Au ($L\alpha_2$), respectively. Particularly, the most prominent peak in Fig. 3 is located at 1.807 keV, which can be contributed to the combined contributions from Si($K\alpha_1$) peaking at 1.739 keV, Si($K\alpha_2$) peaking at 1.740 keV, Sr($L\alpha_1$) peaking at 1.807 keV, Sr($L\alpha_2$) peaking at 1.805 keV, and Sr($L\beta_1$) peaking at 1.872 keV. The EDX spectra of $SrSiO_3:Dy^{3+}$ confirms that the phosphor is composed of Sr, Si, O and Au. The Au element in the specimen was introduced in the process of Au sputtering for the SEM and elemental analyses. However, the characteristic X-ray emissions of Dy^{3+} ions are not detected in $SrSiO_3$ due to the low detection sensitivity of the X-ray analyzer in the EDX facility.

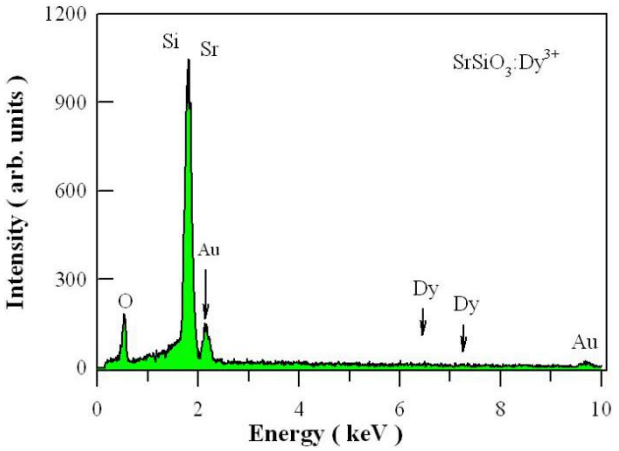

Fig. 4 EDX of Dy^{3+} doped $SrSiO_3$.

3.4 PL of $SrSiO_3:Dy^{3+}$

Upon the 325 nm photoexcitation, the as–prepared $SrSiO_3:Dy^{3+}$ gives off intense visible light emissions. The PL spectrum of the as–prepared $SrSiO_3:Dy^{3+}$ with 5 mol% Dy^{3+} concentration are shown in Fig. 5. All the Dy^{3+} doped samples with different host materials have similar spectral shape, since both the excitation and the emission spectra comprise the characteristic lines of Dy^{3+} within $4f^9$ configuration. The emission spectrum is composed of two groups of emissions peaking at 484 and 575 nm, which can be assigned to the 4f→4f transitions $^4F_{9/2}\rightarrow{}^6H_{15/2}$ and $^4F_{9/2}\rightarrow{}^6H_{13/2}$ of Dy^{3+} ions, respectively [2–4,7,8,16]. Notice that the red emission is less intense than the blue and green emissions. It is well known that the $^4F_{9/2}\rightarrow{}^6H_{13/2}$ transition is hypersensitive and therefore, its intensity strongly depends on the host, while the $^4F_{9/2}\rightarrow{}^6H_{15/2}$ transition is less sensitive to the host [8]. The characteristic emissions of Dy^{3+} in Fig. 5 give evidence on the fact that Dy^{3+} ions act as the luminescence centers of the PL. The inset in Fig. 5 illustrates the PL photo of the as–prepared $SrSiO_3:Dy^{3+}$.

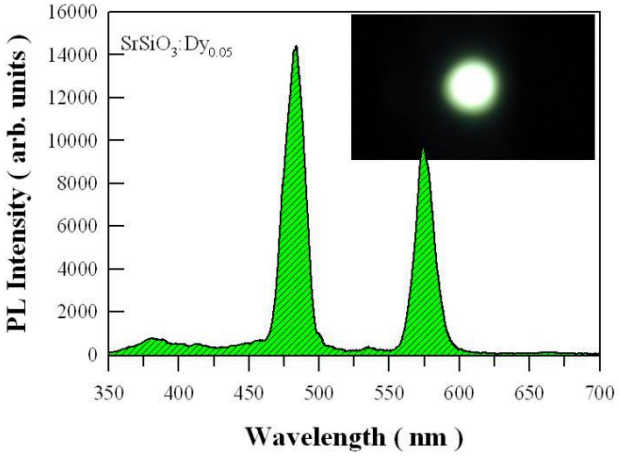

Fig. 5 PL spectra of Dy^{3+} doped $SrSiO_3$. Inset: the PL photos of the as–prepared $SrSiO_3:Dy^{3+}$.

3.5 CIE diagram of Tb doped $SrSiO_3$

Fig. 6 shows the Commission International de l'Eclairage France (CIE) *x–y* color coordinates diagram of the $SrSiO_3:Dy^{3+}$ phosphor. The chromaticity coordinates

of this phosphor calculated using the PL data and the interactive CIE software are $x = 0.270$ and $y = 0.315$. It is clear that they are very close to those of the standard white color (0.333,0.333) in the CIE coordinate system.

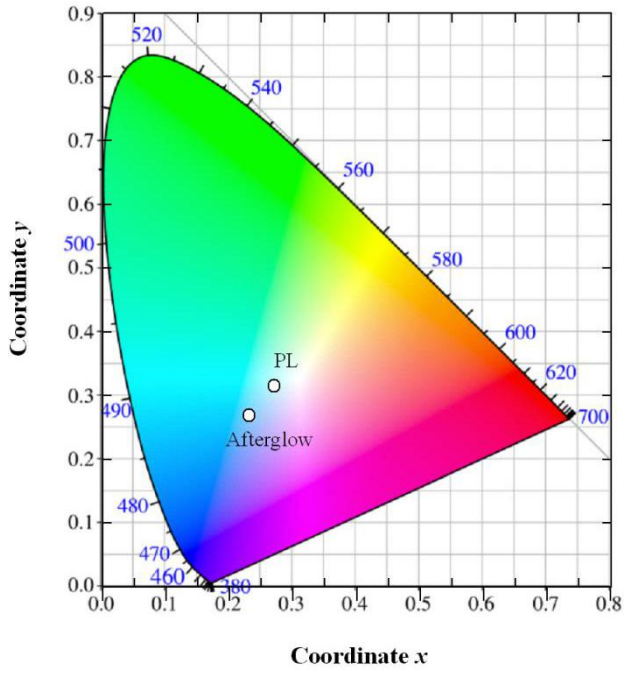

Fig. 6 CIE diagram of the PL from $SrSiO_3:Dy^{3+}$

3.6 Green afterglow of Dy^{3+} doped $SrSiO_3$

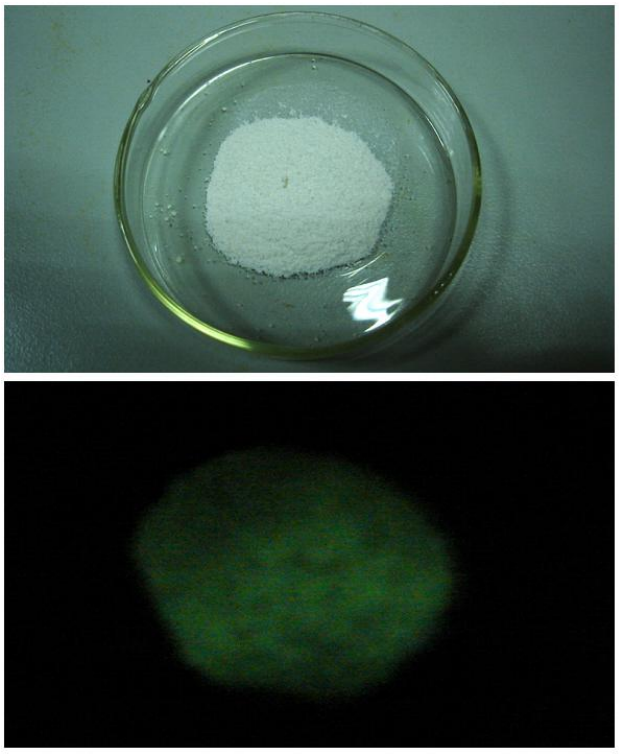

Fig. 7 Photographs of $SrSiO_3:Dy^{3+}$: (a) under room light illumination; (b) after the irradiation of 175 W high–pressure mercury lamp for 10 min.

When the 325 nm irradiation of the laser was blocked off, no afterglow can be observed from $SrSiO_3:Dy^{3+}$. All the samples investigated have green–coloured long afterglow after irradiation with the low–vapour–pressure mercury lamp (175 W). Fig. 7 represents the typical photographs of the $SrSiO_3:Dy^{3+}$ under room light illumination (a) and after the low–vapour–pressure mercury lamp for 5 min (b). It can be seen in Fig. 7 that afterglow from $SrSiO_3:Dy^{3+}$ is green. Long–lasting phosphorescence from Dy^{3+} was observed with the naked eye (0.32 mcd/m^2) for about 1 h in the dark clearly even after the UV lamp had been turned off. Because the afterglow decay process is largely controlled by the properties of traps in the host, the color of afterglow might be different from its PL colour emissions when the decay processes (i.e., the branching ratio) are changed, although the luminescent center of PL and the luminescent center of afterglow are identical.

The afterglow spectrum is shown in Fig. 8. It seems that the afterglow spectrum is the same as the PL spectrum except for their subdued intensity. The first peak in Fig. 8 is located at 483 nm while the second peak is located at 572 nm. The afterglow spectrum in Fig. 8 demonstrates that the luminescent center of the afterglow is Dy^{3+} ion, which is the same as the luminescent center of the PL. The color mainly comes from the mixture of the Dy^{3+} emissions in blue (480 nm) and in yellow (575 nm) regions, since the red emissions (667 nm) are so weak and can be neglected in the afterglow spectrum. The chromaticity coordinates of this afterglow calculated using the afterglow data in Fig. 8 are $x = 0.231$ and $y = 0.269$ in the CIE coordinate system. The perception color of this afterglow is green, as shown in Fig. 6.

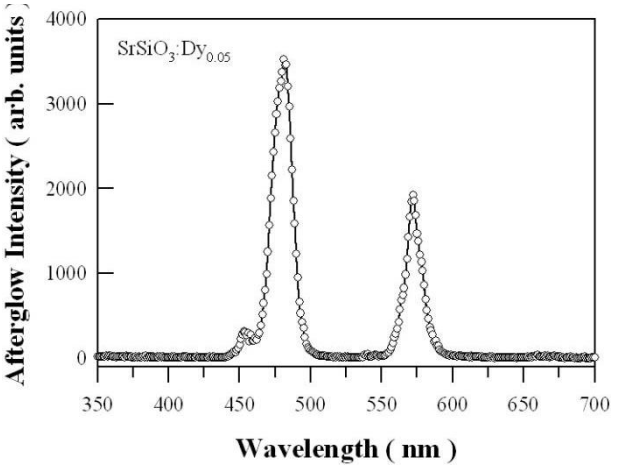

Fig. 8 Afterglow spectra of $SrSiO_3:Dy^{3+}$.

Fig. 9 displays the afterglow decay curve of $SrSiO_3:Dy^{3+}$. The hollow circles represent the experimental afterglow signals. It was found that this decay curve could be best fitted to the two–component exponential function

$$I(t) = I_1 \exp\left(-t / \tau_1\right) + I_2 \exp\left(-t / \tau_2\right) \quad (1)$$

where $I(t)$ is the afterglow intensity at time t after blocking the UV excitation, I_1 is the prefactor of the exponential component whose lifetime decay constant is τ_1, I_2 is the prefactor of the exponential component whose lifetime decay constant is τ_2. The τ_1 extracted from the fitted curve was found to be 24.63 s. Correspondingly, the prefactor I_1 was derived to be 1515.90. Similarly, the τ_2

extracted from the fitted curve was found to be 102.49 s and the prefactor I_2 was derived to be 889.92. The red solid line in Fig. 9 represents the fitting of the experimental signals by the two exponential components with the above–listed parameters. The multiple correlation coefficient, R, and the coefficient of determination, R^2, are both measures of how well the regression model describes the data. In our case, the R is 0.9982 while the R^2 is 0.9964, indicating that the equation is a good description of the relation between the independent and dependent variables.

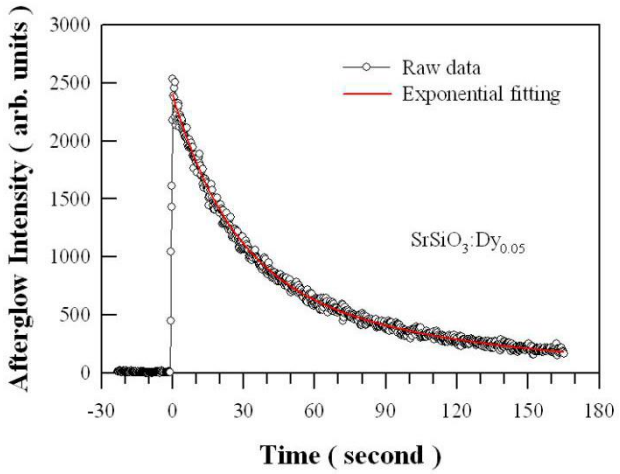

Fig. 9 Afterglow decay curve of $SrSiO_3:Dy^{3+}$.

3.7 Mechanism of the green afterglow of $SrSiO_3:Dy^{3+}$

It is worth noting that the mechanism of the green afterglow of $SrSiO_3:Dy^{3+}$ is quite different from those of Dy^{3+} doped $SrAl_2O_4$, Tb^{3+} doped $SrAl_2O_4$ and Dy^{3+} doped $BaAl_2O_4$ [2–5,7]. In the cases of Dy^{3+} doped $SrAl_2O_4$, Tb^{3+} doped $SrAl_2O_4$ and Dy^{3+} doped $BaAl_2O_4$, their green or blue–green afterglow spectra were a broadband spectrum with its peak centered at around 520 nm or 495 nm, the afterglow centers are suggested to be the intrinsic defects (such as oxygen vacancies) in the host materials. Contrarily, the green afterglow spectrum of $SrSiO_3:Dy^{3+}$ is composed of two sharp peaks with their peaks centered at around 482 and 573 nm, respectively. In the case of $SrSiO_3:Dy^{3+}$, the afterglow centers are the extrinsic defects (i.e., the Dy^{3+} ions) in the host materials. The green afterglow of $SrSiO_3:Dy^{3+}$ casts new light on the afterglow mechanisms of $SrSiO_3$ based phosphors. It is known that defects are generated when Dy^{3+} ions substitute Sr^{2+} sites. As it was reported earlier [2–4,6], Dy^{3+} acts as a supplier of traps by forming defects when it replaces Sr in the crystal. The process can be expressed as follows

$$Dy^{3+} + Sr_{Sr}^{\times} \rightarrow Dy_{Sr}^{\bullet} + Sr_i^{\bullet\bullet} \quad (2)$$

In Eq. (2), the masses, sites and charges are balanced for both intrinsic and extrinsic defects. Eq. (2) indicates that an Dy^{3+} ion substitutes one Sr site in $SrSiO_3$, yielding one positively charged defect $Dy_{Sr}^{\bullet}$ and another positively charged interstitial defect . Thus doping $SrSiO_3$ with Dy^{3+} ions can significantly increase the population density of the defects in the host. When Dy^{3+} doped into $SrSiO_3$ host, due to the chemically $Sr_i^{\bullet\bullet}$ nonequivalent substitution, each substitution of Dy^{3+} ion would create two positive defects. These defects act as trapping centers for charge carriers. If the depth of the trap is too shallow, charge carriers quickly escape from the traps resulting in a fast recombination rate and short lifetime of the afterglow. In our case, Dy^{3+} ions act as a role of creating the electron traps during the high temperature synthesis process. The long–lasting afterglow originates energy transfer from the electron traps to the Dy^{3+} ions, which give birth to the characteristic emissions of Dy^{3+}.

It is interesting to note, however, that we do not get any long–lasting phosphorescence under irradiation by 325 nm laser irradiation, indicating that the long–lasting phosphorescence is not directly rooted in the luminescence of Dy^{3+} ions. However, the Dy^{3+}–doped $SrSiO_3$ phosphors show strong long–lasting afterglow when illuminated with the high–pressure mercury lamp for a couple of minutes. Moreover, the intensity of the afterglow is dependent on the duration of the mercury lamp irradiation. In our case, the green afterglow can be observed with naked eyes in dark room after the mercury lamp irradiation for about 1 min, and the green afterglow reaches its maximal intensity when the phosphor is irradiated for about 5 min. However, the the green afterglow decreases its intensity when the phosphor is irradiated with the mercury lamp for more than 10 min. These observations suggest that the long–lasting afterglow is due to energy transfer from the electron traps to the Dy^{3+} ions.

4. Conclusions

In summary, green afterglow has been observed in $SrSiO_3:Dy^{3+}$ microcrystals synthesized via the high–temperature solid state reaction process at a temperature of 1300 °C. The PL spectrum of $SrSiO_3:Dy^{3+}$ microcrystals is composed of two characteristic blue emission ($^4F_{9/2}\rightarrow{}^6H_{15/2}$) and the yellow emission ($^4F_{9/2}\rightarrow{}^6H_{13/2}$) of Dy^{3+} ions, whose peaks are located at 485 and 572 nm, respectively. Intense green afterglow can be observed from $SrSiO_3:Dy^{3+}$ with naked eyes under the illumination of a high–pressure mercury lamp (175 W) for about 5 minutes. The green afterglow spectrum of $SrSiO_3:Dy^{3+}$ is composed of two sharp peaks with their peaks centered at around 482 and 573 nm, respectively. The PL and afterglow investigations have indicated that the luminescent center of PL is the same as the luminescent center of afterglow for $SrSiO_3:Dy^{3+}$. The afterglow decay curve of the $SrSiO_3:Dy^{3+}$ phosphor exhibits a double exponential decay feature with τ_1 = 24.63 s and τ_2 = 102.49 s. The characteristic features of the green afterglow have indicated that energy transfer from the electron traps to the Dy^{3+} ions.

Acknowledgment

This work was financially supported by Natural Science Foundation of China under the Grant No 11574036.

References

[1] T. Matsuzawa, Y. Aoki, N. Takeuchi, Y. Murayama, A new long phosphorescent phosphor with high brightness, *J. Electrochem. Soc.* 143 (1996) 2670–2673.

[2] Y.M. Huang, Q.L. Ma, Long afterglow of trivalent dysprosium doped strontium aluminate, *J. Lumin.* 160 (2015) 271–275.

[3] Q.L. Ma, B.G. Zhai, Y.M. Huang, Effect of sol–gel combustion temperature on the luminescent properties of trivalent Dy doped $SrAl_2O_4$, *Ceram. Int.* 41 (2015) 5830–5835.

[4] B.G. Zhai, L. Yang, Q.L. Ma, X. Liu, Y.M. Huang, Mechanism of the prolongation of the green afterglow of $SrAl_2O_4:Dy^{3+}$ caused by the use of H_3BO_3 flux, *J. Lumin*. 181 (2017) 78–87.

[5] B.G. Zhai, Y.M. Huang, Green photoluminescence and afterglow of Tb doped $SrAl_2O_4$, *J. Mater. Sci.* 52 (2017) 1813–1822.

[6] B. Qu, B. Zhang, L. Wang, R. Zhou, X.C. Zeng, Mechanistic study of the persistent luminescence of $CaAl_2O_4$:Eu,Nd, *Chem. Mater.* 27 (2015) 2195–2202.

[7] B.G. Zhai, Q.L. Ma, R. Xiong, X. Li, Y.M. Huang, Blue–green afterglow of $BaAl_2O_4:Dy^{3+}$ phosphors, *Mater. Res. Bull*. 75 (2016) 1–6.

[8] M.A. Tshabalala, F.B. Dejene, S.S. Pitale, H.C. Swart, O.M. Ntwaeaborwa, Generation of white–light from Dy^{3+} doped Sr_2SiO_4 phosphor, *Physica B* 439 (2014) 126–129.

[9] D. Dutczak, A. Milbrat, A. Katelnikovas, A. Meijerink, C. Ronda, T. Jüstel, Yellow persistent luminescence of $Sr_2SiO_4:Eu^{2+},Dy^{3+}$, *J. Lumin.* 132 (2012) 2398–2403.

[10] Y. Zhu, M. Ge, Factors affecting afterglow properties of red–emitting phosphor $MgSiO_3:Mn^{2+},Nd^{3+}$ for luminescent fiber, *J. Rare Earth.* 31 (2013) 660–664.

[11] X. Qu, L. Cao, W. Liu, G. Su, Preparation and properties of $CdSiO_3$: Mn^{2+}, Tb^{3+} phosphor, *Ceram. Int.* 38 (2012) 1765–1769.

[12] Y. Liu, B. Lei, C. Shi, Luminescent properties of a white afterglow phosphor $CdSiO_3:Dy^{3+}$. *Chem. Mater.* 17 (2005) 2108–2113.

[13] J. Kuang, Y. Liu, J. Zhang, White–light–emitting long–lasting phosphorescence in Dy^{3+}–doped $SrSiO_3$, *J. Solid State Chem.* 179 (2006) 266–269.

[14] F. Nishi, Strontium Metasilicate, $SrSiO_3$, *Acta Cryst.* C 53 (1997) 534–536.

[15] K.I. Machida, G.Y. Adachi, J. Shiokawa, M. Shimada, M. Koizumi, Structure and high–pressure polymorphism of strontium metasilicate, Acta Cryst. B 38 (1982) 386–389.

[16] Y. Chen, X. Cheng, M. Liu, Z. Qi, C. Shi, Comparison study of the luminescent properties of the white–light long afterglow phosphors:$Ca_xMgSi_2O_{5+x}:Dy^{3+}$(x = 1,2,3), *J. Lumin.* 129 (2009) 531–535.